coatings

MDPI

Article

Influence of Rust Inhibitor on the Corrosion Resistance of Reinforcement in Cement Paste with Chloride

Linchun Zhang [1], Ailian Zhang [1], Ke Li [1], Qian Wang [1], Junzhe Liu [2,*] and Hui Wang [3,4,*]

[1] School of Civil Engineering, Sichuan College of Architectural Technology, Deyang 618000, China; zhanglinchun@scac.edu.cn (L.Z.); zhangailian@scac.edu.cn (A.Z.); like@scac.edu.cn (K.L.); wangqian1@scac.edu.cn (Q.W.)
[2] School of Construction Engineering, Qingdao Agricultural University, Qingdao 266000, China
[3] School of Civil and Environmental Engineering, Ningbo University, Ningbo 315000, China
[4] State Key Laboratory of Materials-Oriented Chemical Engineering, Nanjing Tech University, Nanjing 210000, China
* Correspondence: liujunzhe@qau.edu.cn (J.L.); huiwang123@aliyun.com (H.W.)

Abstract: The electrical resistance and polarization effect of cement paste containing reinforcement were tested to research the anti-corrosion properties of steel bars in cement paste. Moreover, the microstructure and composition of passivation film and rust on the steel bars were studied. The water–cement ratio of the cement paste in this study was 0.3, with 0.5% NaCl, 1% $NaNO_2$, and 1% Benzotriazole, and an assembly unit of 0.5% $NaNO_2$ + 0.5% Benzotriazole by mass of cement was added to the cement to provide a chloride environment. X-ray photoelectron spectroscopy (XPS) and scanning electron microscope (SEM) were applied to research the composition of the passivation film and the microstructure of the cement paste, respectively. The results indicated that the samples with the assembly unit of 0.5% $NaNO_2$ + 0.5% Benzotriazole showed the highest electrical resistance and polarization electrical resistance, while the specimens with 1.0% Benzotriazole showed the lowest electrical resistance and polarization electrical resistance. Moreover, the passivation film of steel bars weakened with increasing distance from the surface of the steel bars. Therefore, the corrosion of steel bars becomes more serious with increasing distance. Finally, the influence of the rust inhibitor on the corrosion resistance of steel bars in the specimens decreased in the following order: 0.5% $NaNO_2$ + 0.5% Benzotriazole > 1.0% $NaNO_2$ > 1.0% Benzotriazole.

Keywords: rust inhibitor; electrical resistance; X-ray photoelectron spectroscopy; scanning electron microscope; corrosion resistance

check for updates

Citation: Zhang, L.; Zhang, A.; Li, K.; Wang, Q.; Liu, J.; Wang, H. Influence of Rust Inhibitor on the Corrosion Resistance of Reinforcement in Cement Paste with Chloride. *Coatings* **2021**, *11*, 606. https://doi.org/10.3390/coatings11050606

Academic Editor: Andrea Nobili

Received: 28 April 2021
Accepted: 14 May 2021
Published: 20 May 2021

Publisher's Note: MDPI stays neutral with regard to jurisdictional claims in published maps and institutional affiliations.

Copyright: © 2021 by the authors. Licensee MDPI, Basel, Switzerland. This article is an open access article distributed under the terms and conditions of the Creative Commons Attribution (CC BY) license (https://creativecommons.org/licenses/by/4.0/).

1. Introduction

As a building construction material with high durability, mechanical properties and low price, concrete has been the most widely used construction building material for many years [1–3]. The mechanical properties, durability and inner mechanisms of cement concrete have attracted the attention of scholars [4–7]. However, many problems related to steel bars applied in complex marine environments still remain unsolved.

In coastal cities, construction buildings made of cement concrete are usually exposed to complex environments. When in service in coastal environments, cement concrete is usually subjected to the influence of freeze–thaw cycles and dry and wet alternation from the seawater. Many researchers have directed their attention toward the influence of external erosion of seawater on the attenuation of mechanical properties and the durability of cement concrete. However, little attention has been paid to the influence of inner salt (for example, the use of sea sand) on the durability of cement concrete [8–12]. It is well known that cement concrete applied in real construction environments are usually reinforced with steel bars. The chloride in seawater or sand can easily corrode the passive film of the steel bars, leading to the corrosion of the steel bars. Following reinforcement corrosion, the rust

on the steel bars can induce cracks in the concrete, resulting in concrete damage [13]. As described in Suzuki's research [14], Zinc-Coated Steels corroded seriously when they were applied in corrosive seawater environments. Moreover, as reported in some studies [15–19], the effect on steel bars of the chloride from either seawater or desalting sand can destroy the passive film of the steel bars, accelerating the corrosion of the steel bars.

To prevent steel corrosion and improve the durability of reinforced concrete, many methods have been tried [20–23]. Improving the compactness of concrete can effectively decrease the penetration of salts. However, this demonstrated little beneficial effect when inner salt was applied in cement concrete. Aiming at these problems, rust inhibitors have been applied in cement concrete. Rust inhibitors can be classified into anode corrosion inhibitors and cathode corrosion inhibitors. Anode corrosion inhibitors are able to prevent the corrosion of steel bars by improving the passive film of the steel bars [24,25]. Additionally, cathodic corrosion inhibitors are able to improve the corrosion resistance of the steel bars by forming a layer of adsorption film on the surface of the steel bar [26]. As reported in several studies, single rust inhibitors like $NaNO_2$ and Benzotriazole have been confirmed to protect steel bars from corrosion [27]. Wang et al. [28] pointed out that when a single rust inhibitor of $NaNO_2$ or Benzotriazole was used in steel-bar-reinforced cement paste, a content of 1% was the most favorable for the corrosion resistance of the steel bars. However, little attention has been paid to the influence of the assembly unit of $NaNO_2$ and Benzotriazole on the corrosion resistance of steel bars in cement concrete with the addition of NaCl.

In this paper, the influence of 1% $NaNO_2$, 1% Benzotriazole, and an assembly unit of 0.5% $NaNO_2$ and 0.5% Benzotriazole on the anti-corrosion properties of steel bars in cement paste with NaCl was investigated. The electrical parameters (electrical resistance, electrical resistance time curves, alternating current (AC) impedance method, and Tafel curves) were determined to reflect the degree of corrosion resistance. Moreover, surface chemical methods (X-ray photoelectron spectroscopy and scanning electron microscopy) were applied to study the change in the passive film.

2. Experimental

Raw Materials

Ordinary Portland cement (produced by Hangzhou Haishi Cement Co., Ltd., Hangzhou, China) with a compressive strength of 42.5 MPa was applied in this study. Φ 10 plain round steel bars were used for the corrosion research. The particle passing percentage and the chemical composition of the cement are shown in Tables 1 and 2.

Table 1. Particle passing percentage of the cementitious materials.

Particlesize/μm / Type	0.3	0.6	1	4	8	16	32	64
Cement	0	0.33	2.66	15.01	28.77	46.64	72.73	93.59

Table 2. Chemical composition of the cementitious materials.

Types	Chemical Composition/%								
	SiO_2	Al_2O_3	Fe_2O_3	MgO	CaO	SO_3	R_2O	MnO	H_2O
Cement	20.86	5.47	3.94	1.73	62.23	2.66	0.48	0	0

In this experiment, the water–cement ratio was 0.3. An amount of 0.5% NaCl by mass of cement was added into the cement. The rust inhibitors $NaNO_2$, benzotriazole (BTA) with purities of 99%–100% were applied in this research. Assembly units of 0.5% $NaNO_2$ + 0.5% Benzotriazole, 1.0% $NaNO_2$, and 1.0% Benzotriazole were added to the mixture, respectively.

An NJ-160 cement paste mixer (Chengdu Xinxin Jianke Technology Co., LTD, Chengdu, China) was employed for manufacturing the cement paste. The mixing process can be summarized as follows: Firstly, cement and water were added into the pot of the NJ-160A cement paste mixer and agitated at 140 rpm for 2 min, and then all mixtures were agitated at 285 rpm for another 2 min. Finally, all of the fresh paste was poured into molds smeared with oil in order to form steel-bar-reinforced cement paste. Samples with dimensions of 50 mm × 50 mm × 50 mm were used to study the electrical properties of the reinforced cement paste. A steel bar possessing a length of 6 cm was embedded in each specimen. A 316L stainless-steel mesh and the steel bar served as the two electrodes for each specimen, with the space between the steel mesh and the axis of the steel bar being 40 mm.

Meanwhile, specimens with dimensions of 40 mm × 40 mm × 160 mm were used to study the composition and microstructure. A steel bar with a size of Φ 10 mm × 2 mm was embedded in each specimen, as shown in Figure 1. The surface rust of all steel bars was removed using abrasive paper, and they were polished with 10% ammonium citrate solution. A TH2810D LCR digital electric bridge (Fuzhou Zhuokai Electronic Technology Co., LTD, Fuzhou, China) was applied to measure electrical resistance, as shown in Figure 2. Alternating voltage and frequency were 1 V and 10 kHz, respectively. Moreover, a direct current (DC) power supply and an ADAM data acquisition system were used to study electric polarization, as shown in Figure 2. The electrical voltage of the DC power supplied in this study was 1 V. An ADAM data acquisition system was used to collect the DC voltage of the samples after they had been maintained under standard curing conditions for a year. The regularity of variation of DC voltage with testing time was investigated. The AC electrical resistance of each specimen was tested once per month, for a period of a year. A TH2810D LCR digital electric bridge (Changzhou Tonghui Co., Ltd., Changzhou, China) with a testing frequency between 100 Hz and 10 kHz was used to test the specimens' AC electrical resistance. An electrochemical workstation (Shanghai Princeton Instrument Co., LTD, Shanghai, China) was used to test the electrochemical impedance spectroscopy. X-ray photoelectron spectroscopy (XPS, Shenzhen Zhuomao Technology Co., LTD, Shenzhen, China) and scanning electron microscopy (SEM, Chongqing Overview Technology Co., LTD, Chongqing, China) were used to investigate the composition and microstructure of the passive film and the rust, respectively, on the reinforcing bar in the cement paste. Moreover, the composition and microstructure of the passive film were determined after 28 days of standard curing. Additionally, the composition and microstructure of the rust were determined after a year of standard curing.

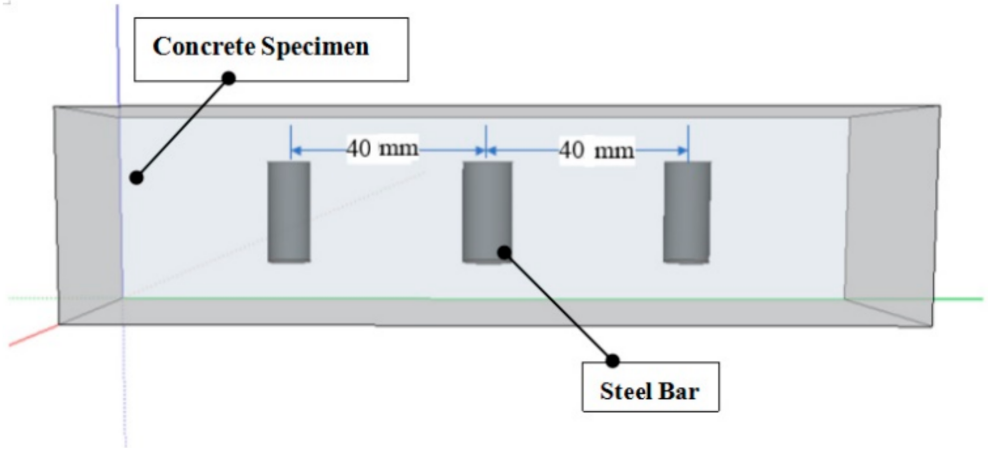

Figure 1. Samples embedded with three steel bars.

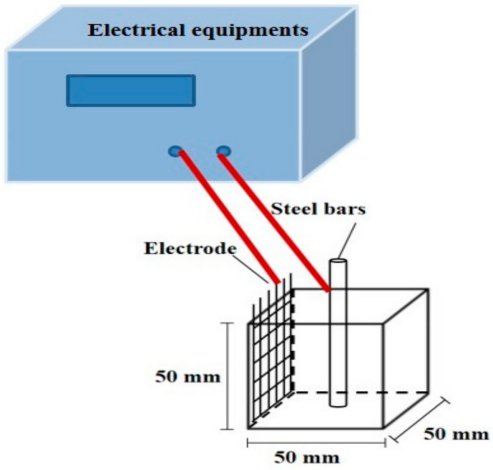

Figure 2. Measurement of electrical parameters.

3. Results and Discussion

3.1. Electrical Performance

Figure 3 shows the variation of AC electrical resistance with increasing curing age. As shown in Figure 3, the electrical resistance of the samples increased with increasing curing age. The electrical resistance of specimens with the assembly unit consisting of 0.5% $NaNO_2$ + 0.5% Benzotriazole was the lowest, while the electrical resistance of the samples with 1.0% Benzotriazole was the highest. Therefore, the steel bars in sample with the assembly unit of 0.5% $NaNO_2$ + 0.5% Benzotriazole exhibited greater difficulty in losing electrons, leading to a lower increase in electrical resistance. Figure 4 depicts the variation of electrical resistance with increasing curing age. It can be observed from Figure 4 that the electrical resistance of specimens with 1.0% Benzotriazole increased most rapidly, indicating that the samples with 1.0% Benzotriazole were more seriously corroded after one year of standard curing. This was attributed to the fact that the addition of cathodic corrosion inhibitor can help to strengthen the corrosion resistance through physical and chemical adsorption on the surface of passive film, and does not promote the corrosion of steel bars. However, the pitting corrosion of steel bars cannot be decreased using a cathodic corrosion inhibitor. Additionally, the anode rust inhibitor was effective at promoting the density of the passive film [28–32]. Therefore, the concrete with the anode rust inhibitor exhibited a better corrosion resistance effect for the steel bars. Compound rust inhibitors are able to take advantage of the anti-rust effects of both anode and cathode corrosion inhibitors. Hence, the specimens with the compound rust inhibitor exhibited the best corrosion resistance performance.

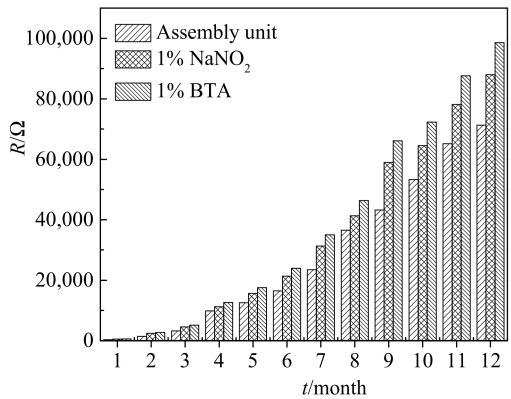

Figure 3. AC electrical resistance with curing age.

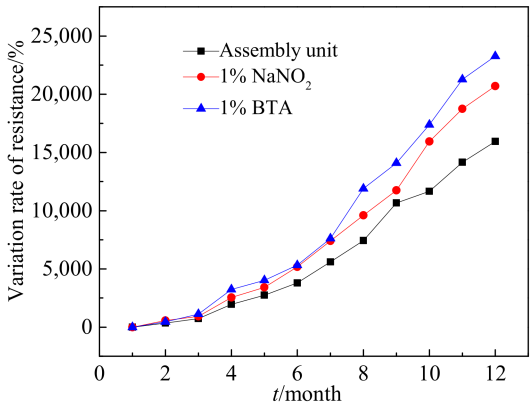

Figure 4. Resistance–time curves of reinforced cement paste.

As has been reported in various studies, when steel bars corrode, the rust on the surface of the steel bars leads to an increase in the capacitive reactance of the steel-bar-reinforced cement paste. The increasing capacitive reactance hinders the migration of electrons [33–36]. Therefore, the cement paste reinforced with the steel bars that corroded more seriously showed higher variation in electrical resistance when direct current was passed through the specimens. Figure 5 shows the resistance evolution–time curves of the specimens after standard curing for a year. The maximum rate of variation for the electrical resistance of the specimens with 1.0% $NaNO_2$, 1.0% Benzotriazole, and the assembly unit of 0.5% $NaNO_2$ + 0.5% Benzotriazole were 6.64%, 37.81%, and 47.28%, respectively. As shown in Figure 5, the specimens with 1.0% Benzotriazole showed the highest polarization resistance. This finding further confirms that the transmission of electrons in steel bars was blocked by the rust on the surface of the steel bars and inside the cement paste when the steel bars were applied in cement paste samples with 1.0% Benzotriazole. Consequently, the steel bars in cement paste with 1.0% Benzotriazole exhibited the most serious corrosion.

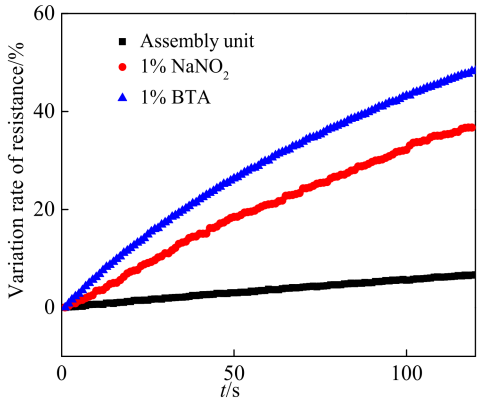

Figure 5. DC electrical resistance–time curves of steel-bar-reinforced cement paste.

The electrochemical impedance spectroscopy (EIS) of the steel-bar-reinforced cement paste is shown in Figure 6. The real part (Z_r) of the steel-bar-reinforced cement paste represents electrical resistance, while the imaginary part (Z_i) represents the electrical reactance. The AC frequency of EIS decreased from 100 kHz to 1 Hz. As reported in previous studies [37–40], when the steel bars in the cement paste corrode, the rust inside the cement paste or on the surface of the steel bars blocks the migration of electrons and increases the electrical resistance of the specimens. Therefore, the real part of the electrochemical impedance spectroscopy that corrodes most seriously will be located on the right side. All specimens were maintained under a standard curing environment for a year. In Figure 6, the electrochemical impedance spectroscopy curves with the addition of the assembly units of 0.5% $NaNO_2$ + 0.5% Benzotriazole, 1.0% Benzotriazole and 1.0%

$NaNO_2$ are presented from left to right, respectively, indicating that the electrical resistance increased in the order of 0.5% $NaNO_2$ + 0.5% Benzotriazole < 1.0% Benzotriazole < 1.0% $NaNO_2$. This was attributed to the fact that the corrosion resistance ability of the steel-bar-reinforced cement paste increased in the order of 1.0% Benzotriazole < 1.0% $NaNO_2$ < 0.5% $NaNO_2$ + 0.5% Benzotriazole. Therefore, rust occurred in the steel bars, eventually leading to decreased electrical conduction in the steel-bar-reinforced cement paste.

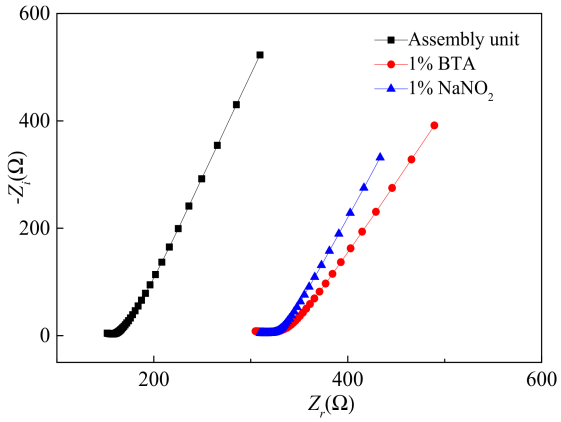

Figure 6. EIS curves of steel-bar-reinforced cement paste.

On the basis of the electrochemical impedance spectroscopy results, the corresponding equivalent circuits of the steel-bar-reinforced concrete are shown in Figure 7. As illustrated in Figure 7, the steel-bar-reinforced cement paste fits the conduction models of four electrical components connected in series. As shown in Figure 7, R_s is the contact electrical resistance between electrodes and specimens. R_1, R_2 and R_3 are the electrical resistances of the pore solution, the cement matrix and the rust, respectively. Meanwhile, C_1, C_2 and C_3 represent the corresponding electrical capacitances. The Chi-squared of each specimen was lower than 1.012×10^{-5}. These results indicated that the equivalent circuit model used for the steel-bar-reinforced cement paste was reasonable.

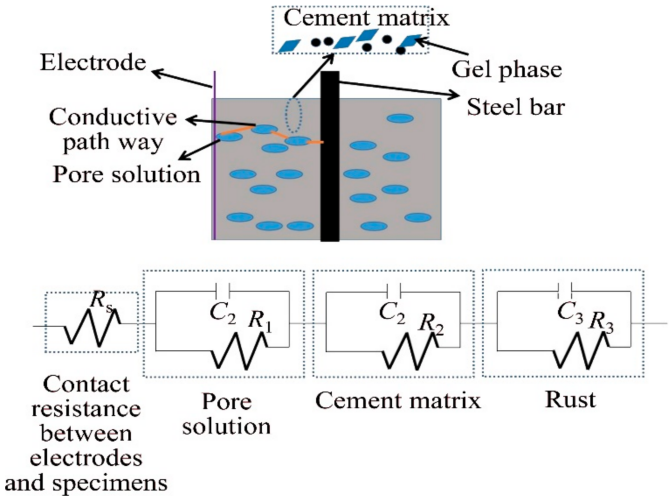

Figure 7. Corresponding equivalent circuits of steel-bar-reinforced cement paste.

3.2. Composition of Passivation Film

Figures 8 and 9 are the XPS scanning full spectrum of the steel passivation film on the surface of the steel bars of the specimens with assembly units of 0.5% $NaNO_2$ + 0.5% Benzotriazole and 1.0% Benzotriazole, respectively. The experiments were carried out after samples had been cured for a year. It can be observed from the figures that the steel

passivation film was mainly composed of iron oxides as well as some complex calcium salts. For the samples with 1.0% Benzotriazole, the diffraction peak intensity of Fe 2p was higher at positions 0 nm and 5 nm away from the surface of the steel bars. However, the diffraction peak intensity of O 1s was the lowest. This indicated that the surface of the steel bars at the position of 5 nm was more seriously. As illustrated in Figures 8 and 9, the O 1s of the samples with 1.0% Benzotriazole was higher than that of the samples with the assembly unit of 0.5% $NaNO_2$ + 0.5% Benzotriazole.

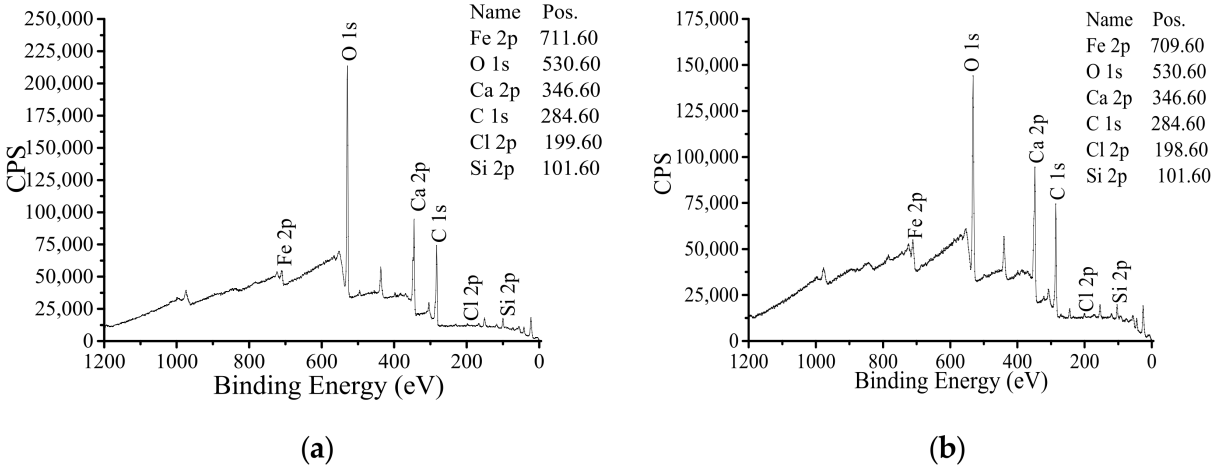

Figure 8. XPS scanning full spectrum of the rust on the steel bars (1.0% Benzotriazole): (**a**) 0 nm away from the surface of the steel bars, (**b**) 5 nm away from the surface of the steel bars.

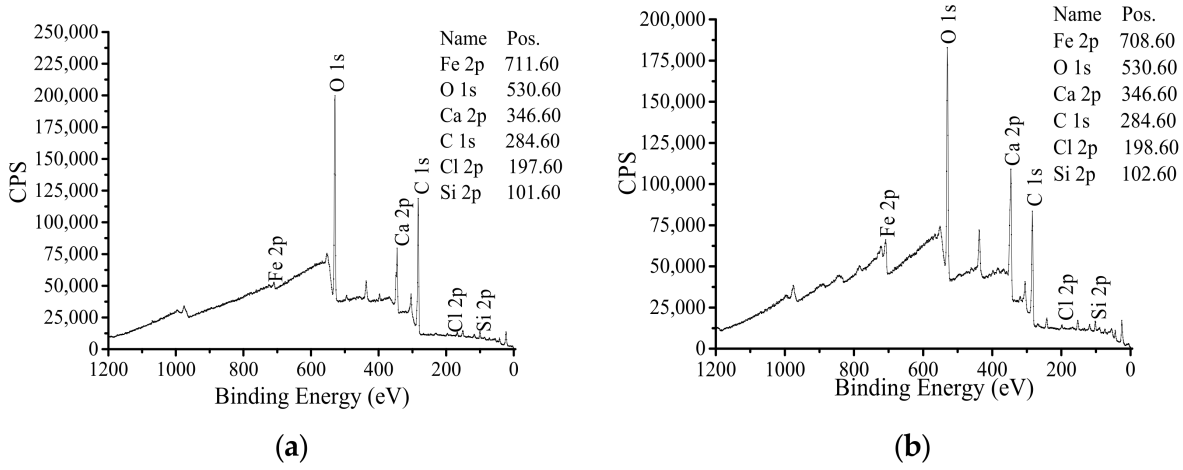

Figure 9. XPS scanning full spectrum of the rust on the steel bars (0.5% $NaNO_2$ + 0.5% Benzotriazole): (**a**) 0 nm away from the surface of the steel bars, (**b**) 5 nm away from the surface of the steel bars.

Figures 10 and 11 show the peak fitting curves of the XPS of the specimens with assembly units of 0.5% $NaNO_2$ + 0.5% Benzotriazole and 1.0% Benzotriazole, respectively. As described in Figures 1 and 10, the rust on the surface and inner layers of the steel bars was mainly composed of FeO and FeOOH, while only a small amount of Fe_3O_4 was present in the rust. The content of FeO, FeOOH and Fe_3O_4 at the position of 0 nm was lower than that at the position of 5 nm. Moreover, the steel bars in cement paste with 1.0% Benzotriazole exhibited a higher iron oxide content than the specimens with 0.5% $NaNO_2$ + 0.5% Benzotriazole.

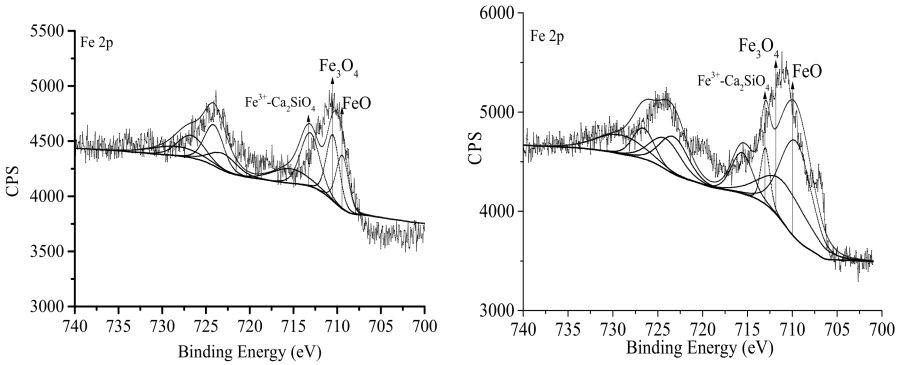

Figure 10. XPS scanning full spectrum of the rust on the steel bars (0.5% $NaNO_2$ + 0.5% Benzotriazole): (**a**) 0 nm away from the surface of the steel bars, (**b**) 5 nm away from the surface of the steel bars.

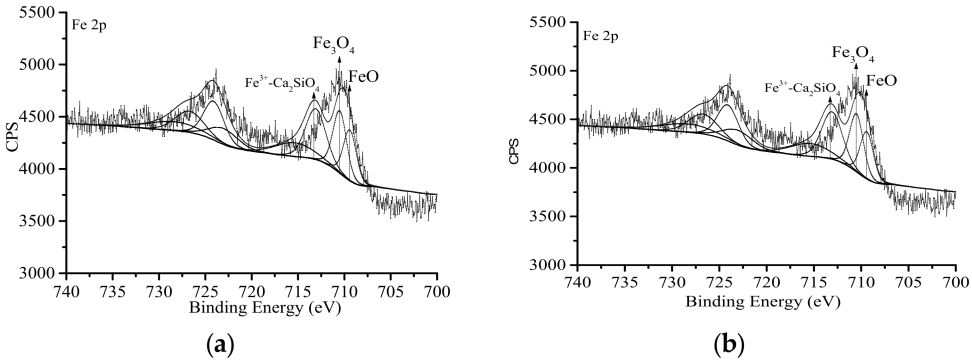

Figure 11. XPS scanning full spectrum of the rust on the steel bars (1.0% Benzotriazole): (**a**) 0 nm away from the surface of the steel bars, (**b**) 5 nm away from the surface of the steel bars.

Figure 12 shows the SEM micrographs of the specimens with 0.5% $NaNO_2$ + 0.5% Benzotriazole and 1.0% Benzotriazole. As shown in Figure 12, the hydration structure of the specimen with 0.5% $NaNO_2$ + 0.5% Benzotriazole was more compact than that with 1.0% Benzotriazole. This indicated that chloride ions penetrated easily into the cement paste with 1.0% Benzotriazole. Additionally, more cracks formed when load was applied to the specimen with 1.0% Benzotriazole. Therefore, the specimen with 0.5% $NaNO_2$ + 0.5% Benzotriazole presented better corrosion resistance.

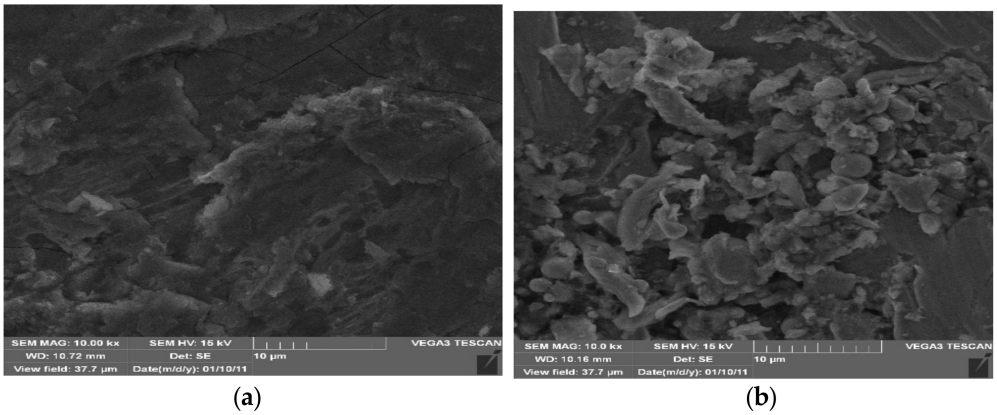

Figure 12. SEM micrographs of specimens: (**a**) 0.5% $NaNO_2$ + 0.5% Benzotriazole, (**b**) 1.0% Benzotriazole.

4. Conclusions

In this work, we investigated the effect of rust inhibitors on the electrical properties of steel-bar-reinforced cement paste. The anti-corrosion mechanisms were confirmed on the basis of characterizations of the composition and structure of the passivation film and rust on steel bars. On the basis of electrical resistance and polarization electrical resistance tests, we demonstrated that the specimen with 0.5% $NaNO_2$ + 0.5% Benzotriazole possessed the best corrosion resistance. Based on the results of electrochemical impedance spectroscopy, the conduction mechanism of steel-bar-reinforced cement paste can be summarized as corresponding to that of four electrical elements in series. The microstructure characterizations implied that rust inhibitors are able to simultaneously influence the structure of steel bars and cement pastes. For steel bars, the samples with 0.5% $NaNO_2$ + 0.5% Benzotriazole exhibited the least degradation of the passivation film. However, when embedded in samples with 1.0% Benzotriazole, the steel bars displayed the most serious corrosion. Additionally, a more porous structure of the cement matrix can be induced using 1.0% Benzotriazole, further degrading the durability of the samples. All these results highlight the importance of the selection and dosage of rust inhibitors in improving anti-corrosion properties and paving the way for the design of reinforced concrete with improved durability.

Author Contributions: Data curation, L.Z., K.L., Q.W. and H.W.; Funding acquisition, L.Z. and J.L.; Investigation, L.Z., A.Z., Q.W. and H.W.; Methodology, A.Z.; Project administration, J.L.; Resources, K.L. and H.W.; Software, A.Z.; Supervision, A.Z. and K.L.; Validation, A.Z. and K.L.; Writing—original draft, H.W.; Writing—review & editing, L.Z., J.L. and H.W. All authors have read and agreed to the published version of the manuscript.

Funding: This work was sponsored by the National Natural Science Foundation of China [No.51808300, No.51778302], Natural Science Foundation of Ningbo [No. 2018A610357] and K.C. Wong Magna Fund in Ningbo University.

Institutional Review Board Statement: Not applicable.

Informed Consent Statement: Not applicable.

Data Availability Statement: Not applicable.

Conflicts of Interest: The authors declare no conflict of interest.

References

1. He, B.; Gao, Y.; Qu, L.; Duan, K.; Zhou, W.; Pei, G. Characteristics analysis of self-luminescent cement-based composite materials with self-cleaning effect. *J. Clean. Prod.* **2019**, *225*, 1169–1183. [CrossRef]
2. Mo, Z.; Gao, X.; Su, A. Mechanical performances and microstructures of metakaolin contained UHPC matrix under steam curing conditions. *Constr. Build. Mater.* **2021**, *268*, 121112. [CrossRef]
3. Zhang, J.; Chen, T.; Gao, X. Incorporation of self-ignited coal gangue in steam cured precast concrete. *J. Clean. Prod.* **2021**, *292*, 126004. [CrossRef]
4. Ren, G.; Yao, B.; Huang, H.; Gao, X. Influence of sisal fibers on the mechanical performance of ultra-high performance concretes. *Constr. Build. Mater.* **2021**, *286*, 122958. [CrossRef]
5. Yang, J.; Huang, J.; Su, Y.; He, X.; Tan, H.; Yang, W.; Strnadel, B. Eco-friendly treatment of ow-calcium coal fly ash for high pozzolanic reactivity: A step towards waste utilization in sustainable building material. *J. Clean. Prod.* **2019**, *238*, 117962. [CrossRef]
6. He, X.; Zheng, Z.; Ma, M.; Su, Y.; Yang, J.; Tan, H.; Wang, Y.; Strnadel, B. New treatment technology: The use of wet-milling concrete slurry waste to substitute cement. *J. Clean. Prod.* **2020**, *242*, 118347. [CrossRef]
7. Liu, X.; Ma, B.; Tan, H.; Gu, B.; Zhang, T.; Chen, P.; Li, H.; Mei, J. Effect of aluminum sulfate on the hydration of Portland cement, tricalcium silicate and tricalcium aluminate. *Constr. Build. Mater.* **2020**, *232*, 117179. [CrossRef]
8. Tan, H.; Zhang, X.; He, X.; Guo, Y.; Deng, X.; Su, Y.; Yang, J.; Wang, Y. Utilization of lithium slag by wet-grinding process to improve the early strength of sulphoaluminate cement paste. *J. Clean. Prod.* **2018**, *205*, 536–551. [CrossRef]
9. Zhang, G.; Yu, H.; Li, H.; Yang, Y. Experimental study of deformation of early age concrete suffering from frost damage. *Constr. Build. Mater.* **2019**, *215*, 410–421. [CrossRef]
10. Zou, F.; Tan, H.; Guo, Y.; Ma, B.; He, X.; Zhou, Y. Effect of sodium gluconate on dispersion of polycarboxylate superplasticizer with different grafting density in side chain. *J. Ind. Eng. Chem.* **2017**, *55*, 91–100. [CrossRef]
11. Shi, X.; Fay, L.; Peterson, M.M.; Yang, Z. Freeze–thaw damage and chemical change of a portland cement concrete in the presence of diluted deicers. *Mater. Struct.* **2009**, *43*, 933–946. [CrossRef]

12. Xu, W.; Lo, Y.T.; Ouyang, D.; Memon, S.A.; Xing, F.; Wang, W.; Yuan, X. Effect of rice husk ash fineness on porosity and hydration reaction of blended cement paste. *Constr. Build. Mater.* **2015**, *89*, 90–101. [CrossRef]
13. Al-Sibahy, A.; Sabhan, M. Corrosion effects on the bond behaviour of steel bars in self-compacting concrete. *Constr. Build. Mater.* **2020**, *250*, 118568. [CrossRef]
14. Suzuki, Y.; Morishita, A. Influence of corrosion inhibitor in chemical conversion coatings on corrosion performance in scratches in zinc-coated steels. *ISIJ Int.* **2019**, *59*, 1878–1885. [CrossRef]
15. Zhou, Z.; Ma, W.; Zhang, S.; Mu, Y.; Li, G. Effect of freeze-thaw cycles in mechanical behaviors of frozen loss. *Cold Reg. Sci. Technol.* **2018**, *146*, 9–18. [CrossRef]
16. Etteyeb, N.; Dhouibi, L.; Takenouti, H.; Triki, E. Protection of reinforcement steel corrosion by phenylphosphonic acid pre-treatment PART II: Tests in mortar medium. *Cem. Concr. Compos.* **2016**, *65*, 94–100. [CrossRef]
17. Ba, M.-F.; Qian, C.-X. Hydration evolution of pre-cast concrete with steam and water curing. *J. Cent. South Univ.* **2013**, *20*, 2870–2878. [CrossRef]
18. Paul, G.; Boccaleri, E.; Buzzi, L.; Canonico, F.; Gastaldi, D. Friedel's salt formation in sulfoaluminate cements: A combined XRD and 27 Al MAS NMR study. *Cem. Concr. Res.* **2015**, *67*, 93–102. [CrossRef]
19. Wu, Z.; Shi, C.; Khayat, K. Influence of silica fume content on microstructure development and bond to steel fiber in ultra-high strength cement-based materials (UHSC). *Cem. Concr. Compos.* **2016**, *71*, 97–109. [CrossRef]
20. Hilke, V.; Herman, T.; De Graeve, I. Inhibitor evaluation in different simulated concrete pore solution for the protection of steel rebars. *Constr. Build. Mater.* **2016**, *124*, 887–896.
21. Cheewaket, T.; Jaturapitakkul, C.; Chalee, W. Initial corrosion presented by chloride threshold penetration of concrete up to 10 year-results under marine site. *Constr. Build. Mater.* **2012**, *37*, 693–698. [CrossRef]
22. Ormellese, M.; Berra, M.; Bolzoni, F.; Pastore, T. Corrosion inhibitors for chlorides induced corrosion in reinforced concrete structures. *Cem. Concr. Res.* **2006**, *36*, 536–547. [CrossRef]
23. Leon, C.; Val, D. Prediction of corrosion-induced cover cracking in reinforced concrete structures. *Constr. Build. Mater.* **2011**, *25*, 1854–1869.
24. Tang, F.; Lin, Z.; Chen, G.; Yi, W. Three-dimensional corrosion pit measurement and statistical mechanical degradation analysis of deformed steel bars subjected to accelerated corrosion. *Constr. Build. Mater.* **2014**, *70*, 104–117. [CrossRef]
25. Choi, Y.S.; Yi, S.-T.; Kim, M.Y.; Jung, W.Y.; Yang, E.I. Effect of corrosion method of the reinforcing bar on bond characteristics in reinforced concrete specimens. *Constr. Build. Mater.* **2014**, *54*, 180–189. [CrossRef]
26. Kioumarsi, M.M.; Hendriks, M.A.; Kohler, J.; Geiker, M.R. The effect of interference of corrosion pits on the failure probability of a reinforced concrete beam. *Eng. Struct.* **2016**, *114*, 113–121. [CrossRef]
27. Wang, H.; Zhang, A.; Zhang, L.; Liu, J.; Han, Y.; Shu, H.; Wang, J. Study on the influence of compound rust inhibitor on corrosion of steel bars in chloride concrete by electrical parameters. *Constr. Build. Mater.* **2020**, *262*, 120763. [CrossRef]
28. Wang, H.; Zhang, A.; Zhang, L.; Liu, J.; Han, Y.; Wang, J. Research on the influence of carbonation on the content and state of chloride ions and the following corrosion resistance of steel bars in cement paste. *Coatings* **2020**, *10*, 1071. [CrossRef]
29. Torres-Luque, M.; Bastidas-Arteaga, E.; Schoefs, F.; Sánchez-Silva, M.; Osma, J. Non-destructive methods for measuring chloride ingress into concrete: State-of-the-art and future challenges. *Constr. Build. Mater.* **2014**, *68*, 68–81. [CrossRef]
30. Montemor, M.; Alves, J.; Simões, A.; Fernandes, J.; Lourenço, Z.; Costa, A.; Appleton, A.; Ferreira, M. Multiprobe chloride sensor for in situ monitoring of reinforced concrete structures. *Cem. Concr. Compos.* **2006**, *28*, 233–236. [CrossRef]
31. Liu, J.-Z.; Ba, M.-F.; Du, Y.-G.; He, Z.-M.; Chen, J.-B. Effects of chloride ions on carbonation rate of hardened cement paste by X-ray CT techniques. *Constr. Build. Mater.* **2016**, *122*, 619–627. [CrossRef]
32. Maruthapandian, V.; Saraswathy, V.; Muralidharan, S. Development of solid state embeddable reference electrode for corrosion monitoring of steel in reinforced concrete structures. *Cem. Concr. Compos.* **2016**, *74*, 100–108. [CrossRef]
33. Duffoa, G.; Farinab, S.; Giordano, C. Characterization of solid embeddable reference electrodes for corrosion monitoring in reinforced concrete structures. *Electrochim. Acta* **2009**, *54*, 1010–1020. [CrossRef]
34. Qiao, G.; Hong, Y.; Song, G.; Li, H.; Ou, J. Electrochemical characterization of the solid-state reference electrode based on $NiFe_2O_4$ film for the corrosion monitoring of RC structures. *Sens. Actuators B Chem.* **2012**, *168*, 172–177. [CrossRef]
35. Liu, M.; Tan, H.; He, X. Effects of nano-SiO2 on early strength and microstructure of steam-cured high volume fly ash cement system. *Constr. Build. Mater.* **2019**, *194*, 350–359. [CrossRef]
36. Zhang, B.; Tan, H.; Shen, W.; Xu, G.; Ma, B.; Ji, X. Nano-silica and silica fume modified cement mortar used as Surface Protection Material to enhance the impermeability. *Cem. Concr. Compos.* **2018**, *92*, 7–17. [CrossRef]
37. Wang, Q.; Wang, D.; Chen, H. The role of fly ash microsphere in the microstructure and macroscopic properties of high-strength concrete. *Cem. Concr. Compos.* **2017**, *83*, 125–137. [CrossRef]
38. Rivera-Corral, J.; Fajardo, G.; Arliguie, G.; Orozco-Cruz, R.; Deby, F.; Valdez, P. Corrosion behavior of steel reinforcement bars embedded in concrete exposed to chlorides: Effect of surface finish. *Constr. Build. Mater.* **2017**, *147*, 815–826. [CrossRef]
39. El Haleem, S.A.; El Wanees, S.A.; El Aal, E.A.; Diab, A. Environmental factors affecting the corrosion behavior of reinforcing steel. IV. Variation in the pitting corrosion current in relation to the concentration of the aggressive and the inhibitive anions. *Corros. Sci.* **2010**, *52*, 1675–1683. [CrossRef]
40. Gustavo, S.D.; Silvia, B.F. Development of an embeddable sensor to monitor the corrosion process of new and existing reinforced concrete structures. *Constr. Build. Mater.* **2009**, *23*, 2746–2751.